Chinese Chemical Letters 35 (2024) 109124

Contents lists available at ScienceDirect

Chinese Chemical Letters

journal homepage: www.elsevier.com/locate/cclet

Precisely manipulation of core composition of core-shell-type cobalt polyoxoniobates and proton conduction study

Zheng-Wei Guo, Yi Chen, Zhe-Hong Chen, Xin-Xiong Li*, Shou-Tian Zheng*

State Key Laboratory of Photocatalysis on Energy and Environment, School of Chemistry, Fuzhou University, Fuzhou 350108, China

ARTICLE INFO

Article history:
Received 15 July 2023
Revised 22 August 2023
Accepted 18 September 2023
Available online 19 September 2023

Keywords:
Polyoxoniobate
Core-shell
Nanocluster
Atomic-level modulation
Proton conduction

ABSTRACT

The development of core-shell nanoclusters with controllable composition is of utmost importance as the material properties depend on their constituent elements. However, precisely tuning their compositions at the atomic scale is not easily achieved because of the difficulty of using limited macroscopic synthetic methods for atomic-level modulation. In this work, we report an interesting example of precisely regulating the core composition of an inorganic core-shell-type cobalt polyoxoniobate $[Co_{26}Nb_{36}O_{140}]^{32-}$ by controlling reaction conditions, in which the inner Co-core composition could be tune while retaining the outer Nb-shell composition of resulting product, leading to a series of isostructural species with a general formula of $\{Co_{26-n}Nb_{36+n}O_{140}\}$ ($n = 0$–2). These rare species not only can display good powder and single-crystal proton conductivities, but also might provide helpful and atomic-level insights into the syntheses, structures and composition modifications of inorganic amorphous core-shell heterometal oxide nanoparticles.

Core-shell nanostructures have attracted significant interest due to their charming configurations and intercomponent synergistic effects that might enhance their expected functions or launch exotic properties [1–21]. These have rendered the core-shell nanostructures one of prime targets in the development of advanced composite materials. Of them, intensive synthetic efforts have been invested into the development of inorganic core-shell metal nanoparticles during the past decade [1–13]. Precise construction of core-shell species with well-defined molecular structures and compositions is of significance to atomic-level understanding and regulation of their properties. However, although some effective approaches have been explored to precisely control the size, shape, thickness and composition of core-shell metal nanoparticles, it is still an enormous challenge to achieve their atomic-level bonding geometry and structural characterization.

Crystalline inorganic core-shell metal oxide nanoclusters with atomically and geometrically precise structural information are of great interest not only due to their fascinating structural features with unusual physical and chemical properties [22–29], but also important roles as the molecular models for the structures and physicochemical properties of inorganic core-shell metal oxide nanoparticles. Particularly, precisely tuning material compositions at the atomic scale remains an attractive target and scientifically interesting not only for developing novel composite materials with controllable composition but also providing atomic-level insights into the structures and physicochemical properties of amorphous core-shell heterometal nanoparticles.

Nevertheless, the targeted growth of inorganic core-shell heterometal oxide nanoclusters with atomic precision is still beyond our capacity owing to the difficulty of atomic-level design of both core and shell and the complexity of self-assembly reactions. And thus, the development of such species is still being sought, lagged far behind that of inorganic core-shell metal nanoparticles. At present, known such nanoclusters are limited and some representative examples are $Cu_{20}@W_{48}$ [24], $V_6@W_{48}$ [25], $M_{16}@W_{48}$ (M = Fe [26], Al or Ga [27]), $Bi_6@U_{24}$ and $Pb_8@U_{24}$ [28].

Recently, we reported the synthesis of an all-inorganic core-shell-type cobalt polyoxoniobate (PONb) $Na_8K_{14}H_{10}[Co_{26}@Nb_{36}]\cdot nH_2O$ (**1**, $Co_{26}@Nb_{36} = [Co_{26}Nb_{36}O_{140}]^{32-}$), in which a large 36-nuclearity PONb shell $\{Nb_{36}O_{124}\}$ (Nb_{36}) encloses a 26-nuclearity mixed-valence cobalt oxide core $\{Co_{26}O_{32}\}$ (Co_{26}) (Fig. 1) [30]. Interestingly, the core composition of $Co_{26}@Nb_{36}$ is sensitive to the reaction conditions, allowing to precisely tune its inner Co-core content without affecting its outer Nb-shell composition and structure, resulting in a series of isostructures $\{Co_{26-n}Nb_{36+n}O_{140}\}$ ($n = 0$–2). Proton conduction experiments reveal that these materials have good proton conducting properties.

* Corresponding authors.
E-mail addresses: lxx@fzu.edu.cn (X.-X. Li), stzheng@fzu.edu.cn (S.-T. Zheng).

https://doi.org/10.1016/j.cclet.2023.109124
1001-8417/

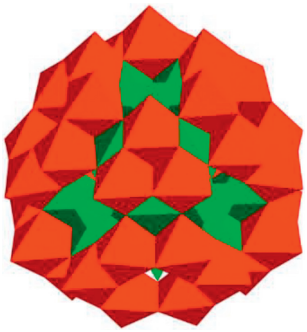

Fig. 1. The polyhedral representation of **1**. CoO_6 octahedra or CoO_4 tetrahedra: green; NbO_6: red.

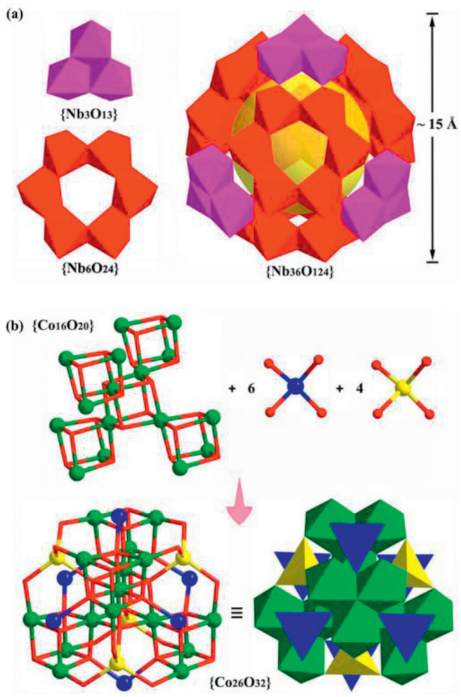

Fig. 2. (a) Polyhedral representation of the sphere-like Nb_{36} nanocage and its two kinds of building units of $\{Nb_3O_{13}\}$ triangle and $\{Nb_6O_{24}\}$ hexagonal ring. (b) An illustration of the structure of the 26-nuclearity Co_{26} core. NbO_6: red or purple; CoO_6 octahedra: green; CoO_4 tetrahedra: yellow or blue.

Solid **1** crystallized in a highly symmetric cubic space group *F*m-3m. The 36-nuclearity Nb_{36} shell structure can be described as a nanosized T_d-symmetry tetrahedral nanocage comprising four $\{Nb_3O_{13}\}$ triangles positioned at its four vertices and four $\{Nb_6O_{24}\}$ hexagonal rings laid flat on its four faces (Fig. 2a), which are interlinked with each other *via* corner-sharing. The 26-nuclearity Co_{26} core, also with T_d-symmetry, contains a tetrahedral $\{Co^{III}{}_{16}O_{20}\}$ core and ten $Co^{II}O_4$ tetrahedra. The $\{Co^{III}{}_{16}O_{20}\}$ core can be seen as consisting of five $Co^{III}{}_4O_4$ cubanes, wherein the innermost $Co^{III}{}_4O_4$ cubane joins four tetrahedrally arranged $Co^{III}{}_4O_4$ cubanes by sharing four Co^{III} atoms (Fig. 2b). Further, the ten $Co^{II}O_4$ tetrahedra occupy the six edge positions (in blue) and the four face-centered positions (in yellow) of the tetrahedral $\{Co^{III}{}_{16}O_{20}\}$ core *via* corner-sharing with $Co^{III}O_6$ octahedra, giving the overall mixed-valence Co_{26} cluster.

Interestingly, the core composition of 1 is markedly affected by the reactants, allowing us to precisely manipulate its Co-core composition with atomic-level precision while keeping the same Nb-shell composition and topology. To begin with, we found that the starting phosphates of Na_3PO_4 and KH_2PO_4 in the reaction of **1** play a key role in determining the resulting core-shell nanocluster with an ordered or disordered core structure though they do not present in the products. Specifically, the reaction of **1** without the addition of phosphates yields an isomorph $Na_{10}K_{15}H_5[NbCo_{25}@Nb_{36}]\cdot nH_2O$ (**2**) ($NbCo_{25}@Nb_{36} = [Co_{25}Nb_{37}O_{140}]^{30-}$). As shown in Fig. 3, the difference between $Co_{26}@Nb_{36}$ and $NbCo_{25}@Nb_{36}$ lies in that the four equivalent Co^{3+} sites (related by a S_4 axis) of the innermost $Co^{III}{}_4O_4$ cubane in the former are found to be occupied either by Nb^{5+} or Co^{3+} ions in the latter. The disordered site is refined freely to give a Co/Nb occupancy factor of 0.758/0.242, followed by fixing it to 0.75/0.25, and thus the core composition of $Co_{25}Nb@Nb_{36}$ is $NbCo_{25}O_{32}$.

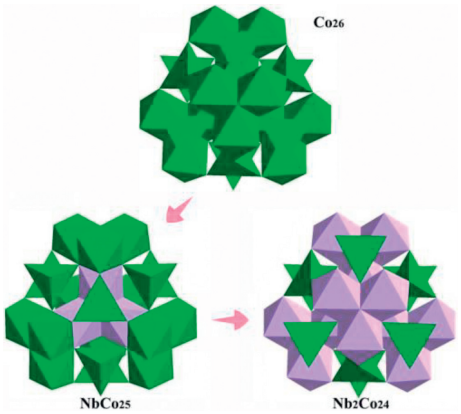

Fig. 3. A comparison of core compositions of Co_{26}, $NbCo_{25}$ and Nb_2Co_{24} in **1**, **2** and **3**, respectively. Ordered CoO_6 octahedra or CoO_4 tetrahedra: green; Disordered MO_6 octahedra: rose.

The observed Nb/Co disorder in $Co_{25}Nb@Nb_{36}$ reveals that Nb and Co ions compete to form the innermost cubane unit in the solution, and the addition of Na_3PO_4 and KH_2PO_4 favors the formation of ordered $Co_{26}@Nb_{36}$. Attempts to obtain analogs of $Co_{26}@Nb_{36}$ proved fruitless by the replacment of the phosphates with nitrate, carbonate, sulfate, acetate or silicate. Considering that core-shell structures are usually grown from inside out, the distinct innermost cubanes of Co_4O_4 and $NbCo_3O_4$ indicate that the starting phosphates Na_3PO_4 and KH_2PO_4 should have a unique influence on the initial nucleation of the core-shell nanocluster. Unfortunately, the detailed role of the phosphates still remains unclear. Potentially, they can affect the competitive relationship between Nb^{5+} and Co^{3+} ions for the initial nucleation of core-shell nanoclusters *via* hydrogen bond interactions or affect the pH value of the reaction solution and thus the reaction and crystallization processes.

Given that Nb and Co ions can compete to form the innermost metal cubane, we set out to explore the molecular growth of the core-shell Co-Nb clusters by adjusting the starting Co/Nb ratio to see if it can affect the core composition of resulting cluster. We studied the Co/Nb ratio influence over the range from 1:9 to 1:1, with the amount of $K_7HNb_6O_{19}\cdot 13H_2O$ fixed at 0.33 mmol. When the Co/Nb ratios are in the range of 1:9∼1:5 (noted that the Co/Nb ratio in the reaction of **2** is about 1:8), the obtained core-shell nanoclusters are all the same as $NbCo_{25}@Nb_{36}$ found in **2**, as confirmed by single-crystal X-ray diffraction analyses of four single crystals from the four same reactions as **2** but with different initial Co/Nb ratios of 1:9, 1:7, 1:6 and 1:5, respectively. Increasing the Co/Nb ratio to 1:4 results in the formation of a new isostructural compound $Na_{10}K_{15}H_3[Nb_2Co_{24}@Nb_{36}]\cdot nH_2O$ (**3**) ($Nb_2Co_{24}@Nb_{36} = [Co_{24}Nb_{38}O_{140}]^{28-}$), in which all trivalent Co^{3+} sites, that is, all Co sites of the whole tetrahedral $\{Co^{III}{}_{16}O_{20}\}$ core in $Co_{26}@Nb_{36}$, are found as disordered Co/Nb sites in

Nb_2Co_{24}@Nb_{36} (Fig. 3). The asymmetric unit of the $\{M_{16}O_{20}\}$ (M stands for disordered Co/Nb sites) core in Nb_2Co_{24}@Nb_{36} contains two crystallographic independent M sites of M1 and M2, which are refined freely to give Co/Nb occupancy factors of 0.789/0.211 and 0.892/0.108, respectively, followed by fixing them to 0.8/0.2 and 0.9/0.1. Since the $\{M_{16}O_{20}\}$ consists of four M1 and twelve M2, its composition exactly is $\{Nb_2Co_{14}\}$. Similar to the bivalent Co^{2+} sites in Co_{26}@Nb_{36} and $NbCo_{25}$@Nb_{36}, all Co^{2+} sites in Nb_2Co_{24}@Nb_{36} are found to be full occupancy. And thus, the overall core composition is Nb_2Co_{24}. We further increased the Co/Nb ratios from 1:3 to 1:1 with attempt to get new isostructres and to check if these tetrahedrally coordinated Co^{2+} sites can be disordered as Co/Nb sites, however, no isostructural species but amorphous phases were obtained.

The distinct inner core compositions make $NbCo_{25}$@Nb_{36} and Nb_2Co_{24}@Nb_{36} nanoclusters have different cluster charges of −30 and −28, respectively. Considering that the only difference in the syntheses of them is the starting amount of $CoCl_2$, we attribute the formation of the distinct isostructures $NbCo_{25}$@Nb_{36} and Nb_2Co_{24}@Nb_{36} to the role of the Co^{2+} ions on the mediation of solution pH *via* hydrolysis. It is known that, in basic solution, a higher solution pH will stabilize a higher-charge polyoxoanion. With different starting Co/Nb ratios from 1:9 to 1:5, the pH values after reactions are about 12.5 ± 0.1 (Table S1 in Supporting information), suggesting the Co/Nb ratios in the range from 1:9 to 1:5 have little effect on the pH values of reactions. Accordingly, all these reactions yield the same nanocluster of $NbCo_{25}$@Nb_{36} with a net charge of −30. While, when the Co/Nb ratio increases to 1:4, the pH value after reaction decreases to 11.9, suggesting that this ratio has an obvious effect on the pH value of reaction. Accordingly, the reaction gives Nb_2Co_{24}@Nb_{36} with a lower net charge (−28) compared to $NbCo_{25}$@Nb_{36}. We can therefore speculate that the hydrolysis of different Co^{2+} concentrations lead to reaction solutions with different pH values, which make *in-situ* generating intermediates adjust their inner core compositions to form isostructural clusters with different negative charges that could be adapted to different pH values of reaction solutions.

The above results reveal that the atomic-level modulation of core-shell Co_{26}@Nb_{36} cluster with order/disorder core structure and programmable core composition can be achieved by controlling the starting reagents. The obtainment of the series of core-shell Co-Nb bimetallic clusters constitutes a family with a general formula of $\{Co_{26-n}Nb_{36+n}O_{140}\}$ (n = 0–2 in this work). These nanoclusters might provide atomic-level insights into the influence of the starting chemicals on the structures and compositions of amorphous bimetallic core-shell nanoparticles. Additionally, the observed disordered core structure evolution from $\{Co_4O_4\}$ to $\{NbCo_3O_4\}$, and to $\{Nb_2Co_{14}O_{20}\}$ provides a case to reveal an inside-out molecular growth of core-shell bimetal nanoclusters at atomic level.

The metal contents of **2**–**3** were determined by ICP analyses, which are in good agreement with the calculated values based on single-crystal X-ray diffraction analyses (Table S2 in Supporting information). Further, XPS were performed to confirm their ratios in **2**–**3** (Fig. S1 in supporting information). Curve-fitting of the high-resolution Co 2p spectra reveals that the Co^{3+}/Co^{2+} ratios in **2**–**3** are 1.48 and 1.38, respectively, perfectly matching their corresponding Co^{3+}/Co^{2+} ratios of 1.50 and 1.40 identified by the BVS calculations [31].

High chemical stabilities, the presence of counter cations (H^+, Na^+, and K^+) and oxo-rich surface point to the possible utility of **1** as proton conducting material. The conductivity of **1** was investigated by ac impedance measurements using a two-electrode configuration between 10^7 and 1 Hz. The humidity-dependent conductivity was first measured at room temperature (RT) (25 °C). As dipicted in Fig. 4a, the conductivity is 2.68×10^{-4} S/cm at 55% relative humidity (RH), and it incerases to 1.74×10^{-3} S/cm when RH maintianed at 98%. Next, the temperature-dependent proton conductivity was measured over the temperature range of 25–85 °C under 98% RH. The result reveal that the conductivity of **1** reaches 2.64×10^{-2} S/cm at 85 °C (Fig. 4b), which is among the highest conductivity reported for POMs (Table S3 in Supporting information). According to the Arrhenius equation $\sigma T = \sigma_0 \exp(-E_a/k_B T)$, the activation energy, determined by linear regression analysis, is estimated to 0.304 eV (Fig. 4c), indicating that conduction is mainly carried out by the "Grotthus" mechanism (E_a < 0.4). We attribute the excellent proton conductivity to the presence of rich proton carriers within the structure of **1**, including water molecules and terminal oxygen atoms, which help to form hydrogen-bonded proton "hopping" networks [32–35]. Additionally, the PXRD patterns showed that the sample remain consistent before and after conduction tests, revealing the integrity of sample **1** (Fig. 4d).

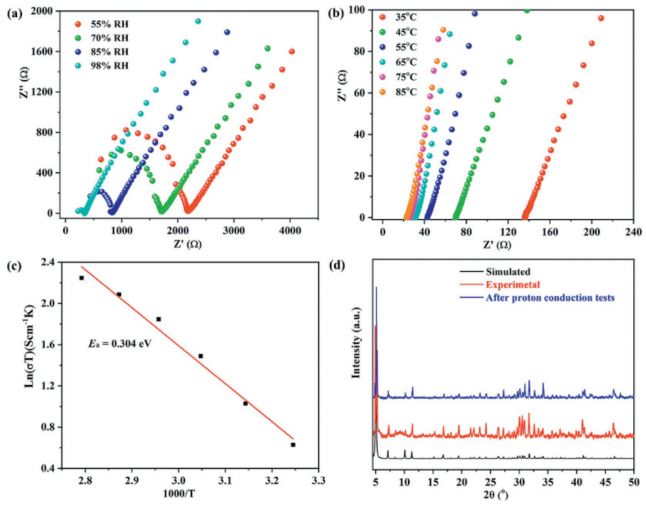

Fig. 4. (a) Nyquist plot for **1** under different relative humidity. (b) Nyquist plot for **1** under different temperatures with 98% RH. (c) Plot of ln(σT) *vs.* 1000/T for **1**. (d) PXRD patterns of **1** before and after tests.

Although extensive research efforts have been devoted to studying the proton-conducting performances of POMs [36–40], most of them are based on compacted crystalline powder samples. The research on the conductivities of single-crystal POMs remains largely unexplored. Given that **1**–**3** contain different amounts of cations and might exhibit distinct conductivities, the single crystal proton conductivities of **1**–**3** were further investigated by ac impedance measurements using single crystals over the temperature range of 35–75 °C under 98% RH. Ag wires were carefully attached to a cubic crystal (0.20 mm × 0.20 mm × 0.20 mm) by using conductive silver paste along opposite faces. The temperature-dependent conductivity measurements reveal that the singel crystal conductivity of **1** at 35 °C is 2.2×10^{-6} S/cm, which is comparable to those of some reported single-crystal POMs [39,40]. As the temperature increases, the conductivity increases gradually and reaches a maximum of 1.08×10^{-5} S/cm at 75 °C (Fig. 5a). The conductivities of **2** and **3** at 35 °C, 75 °C with 98% RH are 1.54×10^{-6} S/cm, 6.84×10^{-6} S/cm and 1.92×10^{-6} S/cm, 5.89×10^{-6} S/cm, respectively (Figs. 5b and c). The results show that the conductivities of **1**–**3** are almost at the same level. Nevertheless, crystal **1** with the most cations shows relatively high conductivity compared to crystals **2** and **3**. According to the Arrhenius equation $\sigma T = \sigma_0 \exp(-E_a/k_B T)$, the activation energy of single crystals **1**–**3**, determined by linear regression analysis, are 0.354, 0.346 and 0.260 eV, respectively, indicating that their conduction processes are mainly dominated by the "Grotthus" mechanism (Fig. 5d).

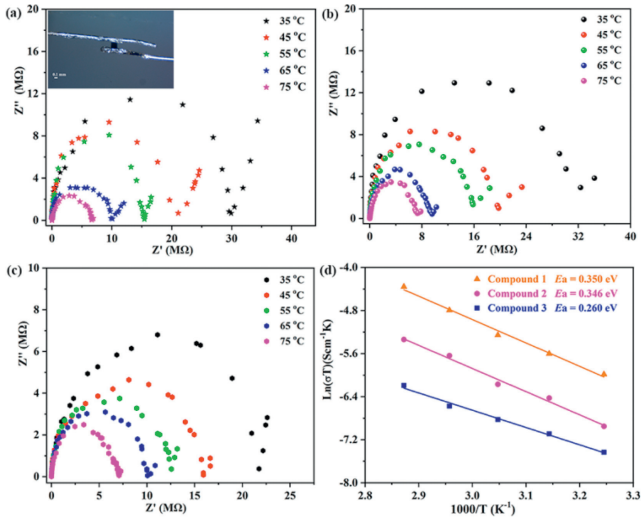

Fig. 5. (a–c) Nyquist plots for single crystals of **1**–**3** under different temperatures with 98% RH, respectively (inset: proton conduction device). (d) Plots of $\ln(\sigma T)$ *vs.* $1000/T$ for single crystals **1**–**3**.

In summary, we demonstrate that the inner core structure (in order/disorder) and composition (with different Co/Nb distributions) of a unique all-inorganic core-shell-type Co-Nb heteropolyoxoniobate $Co_{26}@Nb_{36}$ can be precisely modulated by simple control of initial reaction reagents, leading to a family of isostructural core-shell nanoclusters $\{Co_{26-n}Nb_{36+n}O_{140}\}$ ($n = 0$–2) with precise atoms and structures. Further, their proton conductivities have been examined to showcase them as promising candidates for proton-conducting materials. These bimetallic core-shell structures with tunable core structures allow studies in rich host-guest chemistry to be envisaged. Furthermore, we anticipate that other novel transition metal clusters can be captured, resulting in new discoveries in metal oxo cluster chemistry. Finally, this series of rare all-inorganic and atomically precise Co-Nb core-shell nanoclusters might provide a foundation to understand and investigate the chemical processes of Co-Nb-based non-molecular counterparts including inorganic core-shell nanoparticles and bulk materials.

Declaration of competing interest

The authors declare that they have no known competing financial interests or personal relationships that could have appeared to influence the work reported in this paper.

Acknowledgments

We gratefully acknowledge the financial support from the National Natural Science Foundation of China (Nos. 21971039 and 22171045) and the Key Program of Natural Science Foundation of Fujian Province (No. 2021J02007).

Supplementary materials

Supplementary material associated with this article can be found, in the online version, at doi:10.1016/j.cclet.2023.109124.

References

[1] M. Kitano, Y. Inoue, M. Sasase, et al., Angew. Chem. Int. Ed. 57 (2018) 2648–2652.
[2] X. Cui, W. Li, K. Junge, et al., Angew. Chem. Int. Ed. 59 (2020) 7501–7507.
[3] H. Xiao, B. Liu, L. Qiu, et al., Angew. Chem. Int. Ed. 61 (2022) e202115136.
[4] D.Y. Liu, N.W. Yang, Q. Zeng, et al., Chin. Chem. Lett. 32 (2021) 3288–3297.
[5] H. Dong, L.D. Sun, L.D. Li, et al., J. Am. Chem. Soc. 139 (2017) 18492–18495.
[6] Y. Xiong, Y. Yang, F.J. DiSalvo, H.D. Abruña, J. Am. Chem. Soc. 140 (2018) 7248–7255.
[7] C. Siefe, R.D. Mehlenbacher, C.S. Peng, et al., J. Am. Chem. Soc. 141 (2019) 16997–17005.
[8] G. Liu, W. Zhou, Y. Ji, et al., J. Am. Chem. Soc. 143 (2021) 11262–11270.
[9] S.F. Tan, G. Bisht, U. Anand, et al., J. Am. Chem. Soc. 140 (2018) 11680–11685.
[10] S.T. Hunt, Y. Román-Leshkov, Acc. Chem. Res. 51 (2018) 1054–1062.
[11] Z.W. Qiu, Y.T. Xue, J.Y. Li, et al., Chin. Chem. Lett. 32 (2021) 2807–2811.
[12] Z. Li, R. Wang, J. Xue, et al., J. Am. Chem. Soc. 141 (2019) 17610–17616.
[13] J. Guan, S. Yang, T. Liu, et al., Angew. Chem. Int. Ed. 60 (2021) 21899–21904.
[14] L. Tang, A. Ma, C. Zhang, et al., Angew. Chem. Int. Ed. 60 (2021) 17969–17973.
[15] C. Falaise, S. Khlifi, P. Bauduin, et al., Angew. Chem. Int. Ed. 60 (2021) 14146–14153.
[16] Z. Wang, J.W. Liu, H.F. Su, et al., J. Am. Chem. Soc. 141 (2019) 17884–17890.
[17] J.W. Liu, Z. Wang, Y.M. Chai, et al., Angew. Chem. Int. Ed. 58 (2019) 6276–6279.
[18] J.H. Huang, Y. Si, X.Y. Dong, et al., J. Am. Chem. Soc. 143 (2021) 12439–12444.
[19] S.S. Mal, U. Kortz, Angew. Chem. Int. Ed. 44 (2005) 3777–3780.
[20] A. Mgller, M.T. Pope, A.M. Todea, et al., Angew. Chem. Int. Ed. 46 (2007) 4477–4480.
[21] Z.K. Zhu, Y.Y. Lin, R.D. Lai, et al., Chin. Chem. Lett. 34 (2023) 107773.
[22] K.J. Qin, D.J. Zang, Y.G. Wei, Chin. Chem. Lett. 34 (2023) 107999.
[23] X.F. Fan, W. Pang, H. Feng, et al., Chin. Chem. Lett. 33 (2022) 2783–2798.
[24] Y. Chen, Z.W. Guo, X.X. Li, S.T. Zheng, G.Y. Yang, CCS Chem. 4 (2022) 1305–1314.
[25] Z. Li, Z.H. Lv, H. Yu, et al., CCS Chem. 4 (2022) 2938–2945.
[26] O. Renier, C. Falaise, H. Neal, K. Kozma, M. Nyman, Angew. Chem. Int. Ed. 55 (2016) 13480–13484.
[27] X. Fang, P. Kogerler, Y. Furukawa, M. Speldrich, M. Luban, Angew. Chem. Int. Ed. 50 (2011) 5212–5216.
[28] Z. Li, L.D. Lin, H. Yu, X.X. Li, S.T. Zheng, Angew. Chem. Int. Ed. 57 (2018) 15777–15781.
[29] C. Busche, L. Vilá-Nadal, J. Yan, et al., Nature 515 (2014) 545–549.
[30] Z.W. Guo, L.H. Lin, J.P. Ye, et al., Angew. Chem. Int. Ed. 62 (2023) e202305260.
[31] I.D. Brown, D. Altermatt, Acta Crystallogr. Sect. B Struct. Crystallogr. Cryst. Chem. 41 (1985) 244–247.
[32] B. Tiwari, S. Ram, P. Banerji, ACS Sustain. Chem. Eng. 6 (2018) 16298–16307.
[33] S. Ram, Acta Mater. 49 (2001) 2297–2307.
[34] S. Ram, J. Mater. Sci. 35 (2000) 3561–3571.
[35] S. Ram, Mater. Sci. Eng. A304-306 (2001) 923–927.
[36] H. Ma, B. Liu, B. Li, et al., J. Am. Chem. Soc. 138 (2016) 5897–5903.
[37] Z. Li, X.X. Li, T. Yang, Z.W. Cai, S.T. Zheng, Angew. Chem. Int. Ed. 56 (2017) 2664–2669.
[38] J.C. Liu, Q. Han, L.J. Chen, et al., Angew. Chem. Int. Ed. 57 (2018) 8416–8420.
[39] R. Tsunashima, Y. Iwamoto, Y. Baba, Angew. Chem. Int. Ed. 53 (2014) 11228–11231.
[40] R. Tsunashima, I. Nakamura, R. Oue, et al., Dalton Trans. 46 (2017) 12619–12624.